Full Fault-chain Simulation Study of AC/DC Hybrid Power Grids Considering Sourc-load Meteorological Common-Mode Effects

Yi Wang
State Key Lab of Power Systems
Dept. of Electrical Engineering Tsinghua University
Beijing, China
wang_yi@mail.tsinghua.edu.cn

Zongxiang Lu
State Key Lab of Power Systems
Dept. of Electrical Engineering Tsinghua University
Beijing, China
luzongxiang98@mail.tsinghua.edu.cn

Ying Qiao
State Key Lab of Power Systems
Dept. of Electrical Engineering Tsinghua University
Beijing, China
qiaoying@tsinghua.edu.cn

Xiaobo Wang
State Grid Jiangsu Electric Power Co., Ltd.
Jiangsu, China
wangxb0324@foxmail.com

Dandan Zhu
State Grid Jiangsu Electric Power Co., Ltd.
Jiangsu, China
zdd_life@126.com

Shengjun Wu
State Grid Jiangsu Electric Power Co., Ltd.
Jiangsu, China
wsj333@163.com

***Abstract*— Against the backdrop of accelerating climate change, the core risks of power systems are shifting from conventional internal electrical disturbances to compound, spatiotemporally correlated shocks driven by extreme weather. Focusing on extreme heat, this study develops a source-load meteorological common-mode coupling model and proposes a full fault-chain simulation framework for AC/DC hybrid grids. Using a unified meteorological driver, the model jointly captures the temperature sensitivity of loads and the temperature-derating characteristics of thermal, PV, and wind units, thereby revealing the mechanism of source-load co-deterioration. Simulation studies on the CSEE-VS standard test system using CloudPSS electromagnetic transient analysis show that the spatiotemporal coupling between "latent faults" induced by common-mode effects and explicit AC short-circuit faults can drive the system into instability, whereas either disturbance alone remains recoverable. These results deepen the understanding of weather-driven cascading failures and provide methodological support for dynamic risk analysis of power systems.**

***Index Terms*-- Receiving-end grid, full fault chain, source-load meteorological common-mode, cascading failures.**

I. Introduction

Climate change is driving a shift in the core risks of power systems from conventional internal electrical disturbances to strongly correlated, compound shocks to internal and external factors triggered by extreme weather [1]. China has developed a complex AC/DC hybrid grid characterized by densely located multi-infeed HVDC terminals, highly concentrated receiving-end loads, and large-scale integration of renewable energy sources. This structural evolution extends fault evolution paths from millisecond-scale device actions to second- and minute-scale cross-regional power-flow migrations and protection interactions, thereby forming complex fault chains with strong spatiotemporal coupling [2].

The essence of extreme-weather-induced "*N*-k" contingencies lies in the common-mode effect: a single meteorological hazard can simultaneously weaken multiple components that are spatially correlated but electrically independent [3]. For example, heat waves not only drive up demand, but also overheat transmission and distribution equipment and depress renewable output, causing co-directional degradation across sources, networks, and loads. Such synergistic impacts bypass traditional "*N*-1" assumptions and greatly increase cascading and recovery difficulty [4]. Recent major blackouts in Australia and the UK have confirmed that high-renewable grids face elevated instability risks under extreme weather [5].

Currently, full fault-chain analysis in power systems follows two primary paths [6]. The first comprises power-flow and stability-based approaches that evolve along the lines of self-organized criticality and pattern search, including OPA and its variants [7], hidden-failure models, the Manchester approach [8], CASCADE [9], branching-process models [10], and fault-tree/accident-chain methods [11]. These methods can reveal mechanisms and quantify risk, but they fall short in finely capturing response details and the full evolutionary process [12]. The second path is network-topology-based, integrating complex-network theory with grid structure to trace the structural roots of fault propagation [13]. For AC/DC hybrid-system risk assessment, existing studies largely concentrate on indicator systems, such as branch-reliability assessment frameworks [14], AC/DC-coupling impact factors [15], and dynamic indicators that account for commutation failures and line overloads [16], thereby advancing the field from mechanistic analysis toward practical evaluation [17].

Current meteorology-power studies have progressed from single-factor phenomena to system-level "meteorology-generation-network" coupling, but gaps remain for meteorology-driven full fault chains. First, there is still no

This work was supported by the National Key Research and Development Program of China under the project "Transient Characteristics and Instability Mechanisms of Coupling Interactions Between Large-Scale New Energy and Multi-Infeed HVDC Systems" (Grant No. 2024YFB2408901).

979-8-3315-8138-1

clear system-level characterization of common-mode disturbances in which meteorological conditions act simultaneously on generation and load. Here, "common mode" is extended from electronics to denote a "common pattern" or "synchronous changes"; "source-load-meteorology common mode" refers to the jointly coupled, synchronous variations of generation output, load demand, and meteorological conditions along the source-load-meteorology chain. Second, dynamic coupling models between meteorology and AC/DC hybrid systems remain insufficient, leaving the spatiotemporal linkage from device responses to power-flow redistribution and system stability inadequately captured, and thus limiting engineering-oriented risk assessment. For full-chain failures in receiving-end grids in particular, most existing work still starts from purely electrical disturbances; few studies treat extreme meteorology as a unified exogenous driver that links load escalation and generation derating within a single framework and tracks the ensuing cascading process. This highlights the need to establish a source-load-meteorology common-mode coupling model and to reproduce and characterize its triggering and amplification effects.

Focusing on receiving-end AC/DC hybrid grids under extreme heat, this paper develops a unified meteorology common-mode simulation framework centered on the key mechanism whereby load escalation and generation derating occur synchronously due to "source-load-meteorology common mode." The specific contributions are as follows:

- Established a source-load meteorological common-mode coupling model. Under a unified meteorological input, it simultaneously characterizes the load's temperature response and the temperature-induced derating of thermal power, PV, and wind, and couples them in the same framework with the AC/DC hybrid system, thereby realizing the source-load meteorological common mode.
- Established a full fault-chain simulation paradigm for AC/DC hybrid grids, which accurately reproduces the complete pathway whereby latent faults induced by the "source-load common mode," when coupled with explicit faults such as AC short circuits, ultimately lead to system collapse. This paradigm enables whole-process fault-chain deduction from initial triggering and latent-fault evolution to explicit instability.

The rest of the paper is organized as follow: Section II develops a refined model of the source-load meteorological common-mode, detailing its components and assumptions. Section III couples the common-mode effect with an explicit short-circuit fault to fully reproduce the complete fault-chain process leading to cascading collapse in the power system. Section IV presents the conclusions and outlines directions for future work.

II. Coupling Modeling of Source-Load Meteorological Common-Mode Effects Under Extreme Heat Conditions

Conventional analyses view the impacts of extreme weather on power systems as disturbances to two independent segments: source and load. However, the architecture of modern grids and the wide spatial reach of climate drivers give rise to source-load meteorological common-mode shocks. This chapter builds a meteorology-power system coupling model that explicitly incorporates these common-mode effects to illuminate the systemic risks they pose.

A. Spatiotemporal Meteorological Distribution Model

To represent the spatiotemporal dynamics of extreme heatwaves, we construct a meteorological model that incorporates geographic heterogeneity and diurnal cycles, generating a unified meteorological forcing for source-load coupling via spatial node parameters and stochastic fluctuation terms.

$$T_i(t) = T_{\text{base}} + \Delta T_{\text{global}} + A_i \cdot \sin\left(\frac{2\pi t}{24} + \varphi_i\right) + \varepsilon_i(t) \tag{1}$$

Where, $T_i(t)$ is the ambient temperature at node i and time t ; T_{base} is the baseline temperature; ΔT_{global} is the uniform temperature increase caused by the heatwave; A_i is the diurnal temperature amplitude at node i ; φ_i is the phase offset at node i , reflecting geographic differences; and $\varepsilon_i(t)$ is a stochastic perturbation term that captures small-scale meteorological variability.

B. Load-Temperature Association Model

We decompose the total load into three sectors and build a weather-sensitive model for each. Each model consists of a baseline term, a temperature-sensitive term and a time-distribution function, allowing comparison and superposition within a unified framework.

- Residential load model

Residential demand is the most temperature-sensitive. The model uses a temperature-sensitivity coefficient and a reference temperature to represent the accelerated increase driven by climate-control loads, as follows:

$$P_{\text{res}}(T,t) = P_{\text{base\_res}} \cdot \left[1 + \alpha_{\text{res}} \cdot (T - T_{\text{set}})^2\right] \cdot f_{\text{res}}(t) \tag{2}$$

Where, $P_{\text{res}}(T,t)$ is the residential load at ambient temperature T and time t ; $P_{\text{base\_res}}$ is the baseline residential load; α_{res} is the temperature-sensitivity coefficient for residential load; T is the ambient temperature; T_{set} is the reference setpoint temperature for typical temperature-controlled appliances; and $f_{\text{res}}(t)$ is the residential load time-distribution function.

- Commercial loads

Commercial loads are also affected by temperature, but their response typically demonstrates a linear growth trend. This reflects the steady increase in cooling power demand in public/office spaces. The specific model is as detailed below:

$$P_{\text{com}}(T,t) = P_{\text{base\_com}} \cdot \left[1 + \alpha_{\text{com}} \cdot (T - T_{\text{set}})\right] \cdot f_{\text{com}}(t) \tag{3}$$

Where, $P_{\text{com}}(T,t)$ is the commercial load power at temperature T and time t ; $P_{\text{base\_com}}$ is the base commercial load; α_{com} is the temperature-sensitivity coefficient of the

979-8-3315-8138-1

commercial load; $f_{\text{com}}(t)$ is the time-distribution function of the commercial load.

- Industrial load

Industrial load is primarily driven by production schedules and is less sensitive to short-term temperature fluctuations. It is modeled as a time-dependent baseline load. The specific model is as follows:

$$P_{\text{ind}}(t) = P_{\text{base\_ind}} \cdot f_{\text{ind}}(t) \tag{4}$$

Where, $P_{\text{ind}}(t)$ is the industrial load power at time t ; $P_{\text{base\_ind}}$ is the base industrial load; $f_{\text{ind}}(t)$ is the time-distribution function of the industrial load.

C. Power Generation Unit Output Model

As demand surges, extreme heat simultaneously weakens the peak output of major generation types, forming the other wing of the source-load meteorological common-mode effect. High-temperature derating models are developed for three main sources to reveal the intrinsic causes of power shortages.

- Thermal power units

Using a temperature derating coefficient, we quantify how elevated ambient temperature degrades cold-end efficiency and, in turn, reduces unit output. The specific model is as follows:

$$P_{th}^{max}(T) = P_{th,rated} \cdot \left[1 - \alpha_{th}(T - T_{ref})\right] \tag{5}$$

Where, $P_{th}^{max}(T)$ is the maximum thermal output; $P_{th,rated}$ is the unit's rated capacity at the test temperature T_{ref} ; α_{th} is the thermal-output temperature derating coefficient.

- Distributed photovoltaics

By computing module temperature and correcting with the power temperature coefficient, we capture the PV power decline under "high-temperature with strong irradiance" conditions; the specific model is as follows:

$$P_{pv}(G,T) = P_{STC} \cdot \frac{G}{G_{STC}} \cdot \left[1 - \gamma(T_{cell} - T_{STC})\right] \tag{6}$$

Where, $P_{pv}(G,T)$ is the PV system output at irradiance G and ambient temperature T ; G is the actual irradiance; P_{STC} is the rated power under standard test conditions; G_{STC} is the STC irradiance; γ is the power temperature coefficient; T_{cell} is the PV cell temperature.

- Wind turbines

By applying a temperature correction factor to the standard power curve, we characterize the output derating of wind turbines during hot weather; the specific model is as follows:

$$P_{\text{wind}}(v,T) = P_{\text{wind,rated}}(v) \cdot \left[1 - \alpha \cdot (T - T_{\text{ref}})\right] \tag{7}$$

Where, $P_{\text{wind}}(v,T)$ is the wind-turbine output at wind speed v and temperature T ; $P_{\text{wind,rated}}(v)$ is the rated wind speed-power curve at the standard temperature; α is the temperature influence coefficient; T is the ambient temperature; T_{ref} is the reference temperature.

Under a unified extreme-heat driver, loads rise sharply, generation is derated, and DC systems are also stressed. This source-load co-deterioration initializes a latent fault chain for AC/DC cascading failures, defining the grid's initial vulnerability and seeding subsequent cascading effects.

III. Full Cascading-Failure Analysis Based on Simulation

This paper investigates voltage stability in power systems with high renewable penetration by conducting electromagnetic transient simulations on the CSEE-VS benchmark system using Tsinghua University's CloudPSS platform. Derived from a real grid with over 50% renewable energy, this high-fidelity and authoritative benchmark is well-suited for studying "source-load meteorological common-mode" risks under extreme weather.

TABLE I. Table Type Styles overview of nodes

Voltage level	Number of nodes	Generation type	Rated capacity (MW)
500 kV	20	TP	660×4
220 kV	18	PV	400×3
Below 220 kV	28	WT	400×6
Total	66	HVDC	5000

The CSEE-VS system comprises 66 nodes, forming a 500/220 kV AC/DC main-distribution network with integrated renewable power plants. The total load is 4,905 MW, and the renewable penetration exceeds 50%. Its core is a 20-node 500 kV AC main grid interconnected with the receiving-end system via DC transmission lines. An overview of node locations and voltage levels is given in Table I, and detailed parameters can be found in [18]. For the 40 °C extreme-heat scenario, the simulations focus on key receiving-end buses B01, B02, and B04.

A. Scenario Design and Source-Load Variation

To rigorously quantify the fundamental impact of the source-load-meteorology common mode on power-system security, we construct three progressive scenarios and conduct comparative power-flow analyses:

- Scen.1 (Baseline): Stable operating condition prior to the extreme-heat event.
- Scen.2 (Load-only disturbance): Only the heat-induced demand surge is considered; Load-2 and Load-4 increase markedly while the generation side remains unchanged, isolating the effect of a load-side-only shock.
- Scen.3 (Source-load meteorology common mode): Under extreme heat, system load continues to rise while generation output decreases, reflecting the coordinated meteorological disturbance on both source and load.

The corresponding changes in load and renewable output are compared in Table II and III.

TABLE II. LOAD COMPLEX POWER COMPARISON AND INCREMENTS (SCEN.1: BASELINE; SCEN.2: LOAD DISTURBANCE) UNIT: MW

Load Index	SCEN.1: Baseline	SCEN.2: Load Disturbance	Load Increment	Increment (%)
Load-2	408+j149	530.4 + j163.9	258+j31.4	5.26%
Load-4	452+j165	587.6 + j181.5		

TABLE III. RENEWABLE OUTPUT COMPARISON AND REDUCTIONS (SCEN.1: BASELINE; SCEN.3: SOURCE-LOAD COMMON-MODE) UNIT: MW

Renewable Index	SCEN.1: Baseline	SCEN.3: Common Mode	Renewable Reduction	Reduction (%)
TP	2640	2570.57	69.43	21.88%
PV	1200	1168.44	31.56	
WT	2400	2336.88	63.12	

Table II and III indicate that, under extreme heat, the 5.26% increase in active demand and the 21.88% drop in renewable generation are coordinated responses to the same meteorological driver rather than independent variations. The resulting opposing co-variation of increasing load and decreasing renewable generation constitutes a common-mode effect that produces a power deficit far exceeding that caused by load growth alone and fundamentally reshapes the system power-flow pattern.

B. Power Flow Analysis and Overload Line Identification

Using the loading increase relative to Scen.1 as the screening index, comparison of the three scenarios identifies lines B06-B08, B03-B04, and B05-B03 as the most vulnerable elements under load-only and source-load meteorological common-mode disturbances, as summarized in Table IV.

TABLE IV. LINE COMPLEX POWER ACROSS SCENARIOS UNIT: MW

Line Index	SCEN.1: Baseline	SCEN.2: Load Disturbance	SCEN.3: Common Mode
B06-B08	537.32+j3.52	616.03+j41.81	679.94+j20.32
B03-B04	290.26–j29.17	434.33+j46.76	555.64–j17.02
B05-B03	404.49–j23.85	512.72+j64.97	601.06+j43.84

Table V summarizes line loading for three representative branches across Scenarios 1-3 and their relative increases with respect to the baseline.

TABLE V. LINE LOADING BY SCENARIO AND RELATIVE GROWTH SUMMARY

Line Index	SCEN.1: Baseline	SCEN.2: Load Disturbance	SCEN.3: Common Mode
B06-B08	68.89%	79.16%	87.21%
B03-B04	64.83%	97.08%	123.53%
B05-B03	54.03%	68.91%	80.35%

Under the source-load meteorological common-mode effect, system power flows are strongly redistributed, and the loading of line B03-B04 surges from 64.83% in the baseline to 123.53%, exceeding its thermal limit and triggering protective tripping in the simulations. Although B03-B04 thus evolves from a normal component into a latent-fault element, the resulting static overload and outage do not induce transient instability, but only cause slight bus-voltage fluctuations.

Based on power-flow results for the three scenarios, line loading variations are compared and the most strongly stressed line is selected as the target component for subsequent fault-chain simulations.

C. Full Fault-Chain Evolution under Latent-Manifest Fault Coupling

Scenarios 4-6 are designed to examine how a source-load meteorological common-mode induced latent fault interacts with an additional AC short-circuit on line B03-B04. In each scenario, a fault is applied to B03-B04 at t=5 s and cleared at t=5.09 s, and the resulting voltage transients are compared to assess the impact of this coupling on system stability.

- Scen.4 (Baseline short-circuit): An AC fault occurs in the normal system without meteorological disturbances.
- Scen.5 (Load disturbance and short-circuit): An AC fault occurs under the load-only disturbance scenario.
- Scen.6 (Source-load common-mode and short-circuit): An AC fault occurs while line B03-B04 is already overloaded due to the source-load meteorological common-mode effect.

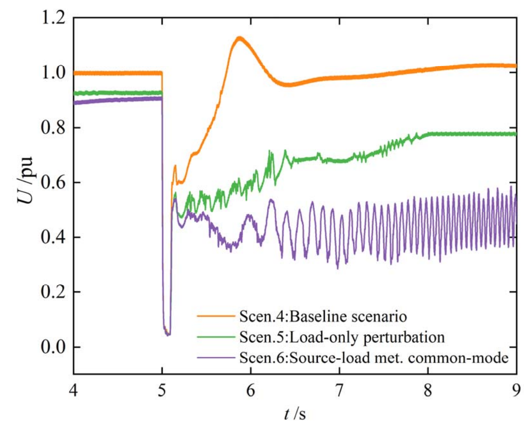

Fig. 1. Comparison of dynamic voltage responses at B03 under different scenarios.

Fig. 1 compares the voltages at bus B03 and highlights distinct stability performance across the three scenarios. Before the AC fault, the baseline case has the highest voltage and the source-load common-mode case the lowest, implying the smallest initial margin in the common-mode case. After fault clearing, the voltage sag becomes deeper and the recovery becomes weaker when moving from the baseline scenario to the load-only disturbance scenario and then to the source-load common-mode scenario, with the common-mode case showing the deepest dip, sustained oscillations, and failure to return to a secure level. The voltage at the WT01 wind turbine bus follows a similar trajectory; the severe depression causes WT01 to violate LVRT requirements and trip offline, further aggravating system risk in the common-mode scenario.

The comprehensive analysis shows that when only the source-load meteorological common-mode effect occurs (Scenario 3), the system merely exhibits power-flow redistribution and line overloading, without triggering a cascading failure. When only a single AC grounding fault occurs (Scenario 4), the system can also fully recover by

979-8-3315-8138-1

virtue of its inherent resilience. However, under the background of a “latent fault” formed by the common-mode effect, the superposition of an otherwise recoverable “explicit” AC fault (Scenario 6) breaks through the system's defensive capability and ultimately induces a cascading failure in the receiving-end grid. This result clearly demonstrates that two individually tolerable and independent faults can, once coupled in space and time to form a “latent-explicit” superposed effect, constitute a complete fault chain sufficient to cause system collapse. By analyzing the fault evolution processes under different scenarios, the study highlights how the latent mechanism of the source-load meteorological common-mode effect, when coupled with an explicit short-circuit fault, can implicitly trigger a full fault chain.

IV. Conclusion

This paper investigates the security and stability of AC/DC hybrid receiving-end grids under extreme heat using a source-load meteorological common-mode coupling model and a full fault-chain simulation framework, revealing how weather-driven “latent-explicit” fault coupling leads to system failure. The main conclusions are:

(1) Extreme-heat-induced source-load meteorological common-mode effects are the root cause of initial system fragility. As a unified external stressor, they simultaneously increase demand and depress generation, aggravating power imbalance and power-flow redistribution, and creating a latent fault background that seeds cascading failures.

(2) The proposed full fault-chain simulation paradigm shows that the spatiotemporal coupling of common-mode-induced latent faults with explicit AC faults is decisive for forming a complete fault chain. Under common-mode-induced line overloading, a short-circuit that would otherwise be tolerable may become unrecoverable because stability margins are eroded, ultimately driving system instability and reproducing the full evolution from meteorological disturbance to collapse.

Future work will further elucidate the coupling and propagation mechanisms of explicit and latent faults under source-load meteorological common-mode conditions, with particular emphasis on quantifying the contributions of different generation units and DC links to the fault current. A deeper investigation into the dynamic interaction processes and the evolution of these faults across multiple time scales will also be undertaken to identify critical risk components.

References

[1] Zhu, Yuanzhen, Wenbo Li, and Yutian Liu. "Propagation model and blackout risk quantitation analysis for cascading failures in AC/DC hybrid power systems." 2019 IEEE Power & Energy Society General Meeting (PESGM). IEEE, 2019.

[2] Mahmood, Hisham, et al. "Dynamic model of back-to-back converter for system-level phasor simulation." 2024 IEEE Power & Energy Society General Meeting (PESGM). IEEE, 2024.

[3] Zheng, Y., Wang, J., Wang, C., Huang, C., Yang, J., & Xie, N. (2025). Strategic bidding of wind farms in medium-to-long-term rolling transactions: A bi-level multi-agent deep reinforcement learning approach. Applied Energy, vol. 383, art. 125265, 2025.

[4] Cho, J., & Papavasiliou, A. (2024). Exact mixed-integer programming approach for chance-constrained multi-area reserve sizing. IEEE Transactions on Power Systems, vol. 39, no. 2, pp. 3310-3323, 2024

[5] Zhang, Yonggang, et al. "Small-Signal AC-DC Coupling Analysis of Grid-Following and Grid-Forming MMCs." 2024 IEEE Power & Energy Society General Meeting (PESGM). IEEE, 2024.

[6] Petersen, Pauli Fridheim, H. Johannsson, and A. H. Nielsen. "Investigation of suitability of cascading outage assessment methods for real-time assessment." IEEE (2015).

[7] Liu, Qin, Tian Liang, and Venkata Dinavahi. "Real-time hierarchical neural network based fault detection and isolation for high-speed railway system under hybrid AC/DC grid." IEEE Transactions on Power Delivery, vol. 35, no. 6, pp. 2853-2864, 2020.

[8] Kumar, Ancha Satish, and Bibhu Prasad Padhy. "Communication-free based decoupled DC-voltage and frequency control in the multi-terminal HVDC (MTDC) grids." 2021 IEEE Power & Energy Society General Meeting (PESGM). IEEE, 2021.

[9] Feng, Wei, et al. "A Joint Sequential State Estimation Algorithm for VSC-MTDC Systems Using Virtual Connections." 2021 IEEE Power & Energy Society General Meeting (PESGM). IEEE, 2021.

[10] Smadi, Abdallah A., et al. "A unified hybrid state estimation approach for VSC HVDC lines embedded in AC power grid." 2023 IEEE Power & Energy Society General Meeting (PESGM). IEEE, 2023.

[11] Collados-Rodriguez, Carlos, et al. "Integration of an MMC-HVDC link to the existing LCC-HVDC link in Balearic Islands based on grid-following and grid-forming operation." IEEE Transactions on Power Delivery, vol. 37, no. 6, pp. 5278-5288, 2022.

[12] Fekri, Mojtaba, Javad Nikoukar, and Gevork B. Gharehpetian. "Vulnerability risk assessment of electrical energy transmission systems with the approach of identifying the initial events of cascading failures." Electric Power Systems Research, vol. 220, art. 109271, 2023

[13] Ye, Xi, et al. "A primary analysis on mechanism of large scale cascading trip-off of wind turbine generators." Automation of Electric Power Systems, vol. 36, no. 8, pp. 11-17, 2012.

[14] Lu, Zongxiang, et al. "Flexibility supply-demand balance in power system with ultra-high proportion of renewable energy." Automation of Electric Power Systems, vol. 46, no. 16, pp. 3-16, 2022.

[15] Wang, Yi, and J. Wu. Energy storage configuration method for distribution networks based on moment difference analysis. Energy, vol. 311, art. 133376, 2024.

[16] Cheng, Tianshi, Ning Lin, and Venkata Dinavahi. "Hybrid parallel-in-time-and-space transient stability simulation of large-scale AC/DC grids." IEEE Transactions on Power Systems, vol. 37, no. 6, pp. 4709-4719, 2022.

[17] Hirsching, Carolin, et al. "On fault-ride-through performance in MMC-HVDC applications controlled as a virtual synchronous machine." IEEE Transactions on Energy Conversion, vol. 37, no. 4, pp. 2803-2812, 2022.

[18] Zhao, Bing, et al. "Benchmark for AC-DC hybrid system with high penetration of renewables (3): voltage stability benchmark CSEE-VS." Proceedings of the Proceedings of the CSEE, vol. 44, no. 21, pp. 8353-8364, 2024.

979-8-3315-8138-1